PCCP

Full-dimensional Quantum Studies of Vibrational Energy Transfer Dynamics between H2O and Ar: Theory Assessing Experiment

Journal:	*Physical Chemistry Chemical Physics*
Manuscript ID	CP-ART-03-2022-001230.R1
Article Type:	Paper
Date Submitted by the Author:	04-May-2022
Complete List of Authors:	Yang, Dongzheng; University of New Mexico College of Arts and Sciences Liu, Lu; Nanjing University, Department of Chemistry and Chemical Engineering Xie, Daiqian; Nanjing University, Department of Chemistry Guo, Hua; University of New Mexico College of Arts and Sciences, Department of Chemistry

Revised, 05/04/2022, submitted, 3/14/2022

Full-dimensional Quantum Studies of Vibrational Energy Transfer Dynamics between H_2O and Ar: Theory Assessing Experiment

Dongzheng Yang,[1] Lu Liu,[2] Daiqian Xie,[2,*] Hua Guo[1,*]

[1] *Department of Chemistry and Chemical Biology, University of New Mexico, Albuquerque, New Mexico 87131, USA*

[2] *Institute of Theoretical and Computational Chemistry, Key Laboratory of Mesoscopic Chemistry, School of Chemistry and Chemical Engineering, Nanjing University, Nanjing 210093, China*

[*]corresponding authors: dqxie@nju.edu.cn, hguo@unm.edu

ABSTRACT

We report the first full-dimensional quantum mechanical calculations of ro-vibrational inelastic scattering dynamics between water molecules and argon atoms on an accurate potential energy surface, using a recently developed time-independent quantum method based on the close-coupling approach. The state-to-state integral cross sections and rate coefficients show strong observance of gap laws. The calculated thermal rate coefficients for the relaxation of stretching fundamental states of H_2O are in good agreement with experimental values, while those for the bending overtone state are approximately five times smaller than the values extracted through a previous kinetic modeling of fluorescence decay data. Our state-specific quantum scattering results suggest the need to reassess the kinetic modeling of the experimental data. This work advanced our understanding of the quantum dynamics of vibrationally inelastic energy transfer processes involving polyatomic molecules.

1. Introduction

Collision-induced energy transfer of molecules with bath species is responsible for a wide array of macroscopic phenomena, such heat and energy transport. It is also a fundamentally important process in many gas-phase chemical environments, such as atmospheric chemistry,[1] combustion,[2] astrochemistry,[3] and chemical lasers.[4] The understanding of the underlying microscopic mechanisms and accurate determination of dynamical properties for such collision processes are of fundamental importance in modeling kinetics in various chemical settings.[5] Because of the quantum nature of molecules, the ultimate understanding requires investigations with quantum state resolution of the collision partners.[6] Theoretically, an accurate characterization of quantum scattering dynamics is very challenging,[7] especially when polyatomic molecules are involved. However, such calculations are necessary to understand fundamental principles in energy transfer and to interpret experimental data. These benchmarks can be further used to validate more approximate models, such as those based on classical[8] and semiclassical methods.[9]

A key issue in quantum state specific energy transfer dynamics is whether the collision is governed by the so-called gap laws. The energy gap law, which stipulates that the transition probability is the largest for energy transfer between initial and final states with roughly the same internal energy,[10] has been observed in many systems.[11-13] Another gap law involves the rotational angular momentum: collisions favor those that conserve the sum of rotational angular momenta of the collision partners.[14] These rules of thumb

hold well in many systems where the collision is governed by repulsive walls, but studies have shown that they break down under certain conditions where strong attractive forces, such as hydrogen bonding, are present.[15, 16]

The vibrational relaxation of the water molecule (H_2O) plays an important role in many gas phase environments, such as the evolution of planetary atmospheres[17] and interstellar media.[3] Combustion often produces a large amount of water vapor.[2] In order to accurately simulate these environments, it is essential to understand the collision dynamics of H_2O with surrounding atoms and molecules. The collision of H_2O with argon (Ar) represents one of such prototypes and has attracted considerable attention. The relevant experimental work on state-resolved kinetics and dynamics began in 1970s with Moore and coworkers, with the first report of the room temperature rate coefficients of quantum state resolved vibrational relaxation by Finzi et al.[18] In this pioneering experiment, single ro-vibrational states belonging to the asymmetric stretching fundamental band of H_2O were first excited by a tunable IR laser, and the decay of several excited vibrational state populations was monitored by fluorescence. A kinetic model was then used to extract the state-specific vibrational relaxation rate coefficients. Subsequently, Hovis and Moore[19] measured the temperature dependence of decay kinetics using the same laser induced fluorescence (LIF) technique and reported the corresponding rate coefficients at a range of temperatures. The rate coefficients for $D_2O(\nu_2)$ relaxation were also measured by Miljanic and Moore.[20] It should be stressed that no state-specific rate coefficient was directly measured in these experiments, because

of restrictions of the experimental setup. Instead, they were extracted through a kinetic model, which involves certain assumptions. Later and independently, Zittel and Masturzo[21] measured the upper limit of vibrational relaxation rate coefficients of H_2O scattered with Ar, N_2, and O_2, from room temperature to 1000 K, and the same kinetic model was used. In 2004, Barnes et al.[22] further reported the rate coefficients for the vibrational relaxation of H_2O from highly excited vibrational states in collisions with H_2O, Ar, H_2, N_2, and O_2.

Theoretical studies of vibrationally energy transfer of this system have significantly lagged behind. So far, the only dynamical calculations for H_2O+Ar vibrational energy transfer were done using a semi-classical method,[23-26] with the H_2O molecule approximated as a harmonic vibrator. The reliability of the results is further compromised by the fact that the interaction between the collisional partners was approximated with empirical functions. In these simulations, only transition probabilities were computed, which were found to be qualitatively consistent with the experimental trend. No quantum dynamics calculation on this system has so far been reported. The lack of the quantum mechanical characterization of the collision dynamics can be attributed to difficulties associated with the full-dimensional quantum treatment of the atom-triatom scattering dynamics. It is only recently that a full-dimensional time-independent quantum mechanical (TIQM) method was developed for the non-reactive scattering between a triatomic molecule and an atom.[16] In this TIQM approach, the close-coupling equations were solved using the eigenfunctions of ro-vibrational states of the polyatomic monomer

as the contracted basis set, which made it feasible to perform the calculations efficiently. This new method has been applied to investigate the inelastic scattering of water molecules with Cl and He.[16, 27] In this work, the H_2O+Ar collision dynamics is characterized by this new TIQM method on a new and accurate potential energy surface (PES) based on high level ab initio data,[28] which yields quantum state specific cross sections and rate coefficients. These quantum results can then be used to assess the approximations made in the kinetic model used to extract state-specific rate coefficients from the LIF experiment.[18, 19, 21] Based on the scattering result, the energy transfer mechanisms and validity of the gap laws are also discussed in detail. This publication is organized as follows. The next section outlines the method, followed by the results and discussion. The final section concludes.

2. Methods

A monomer internal state (MIS) of H_2O, which denotes its ro-vibrational state before or after the scattering process, can be labeled by six quantum numbers $(v_1, v_2, v_3) j_{k_a, k_c}$, for the symmetric stretching (v_1), bending (v_2), antisymmetric stretching (v_3) quantum numbers and the rotational quantum number j as well as its projections k_a and k_c onto the two principal axes. We used the PES developed by Jiang et al.[29] to compute the ro-vibrational eigenstates of H_2O. The details of the bound state calculation can be found in our recent publication[16] and some the low-lying ro-vibrational energies of both the *para*- and *ortho*-H_2O are listed in Table 1.

The full-dimensional interaction PES for the H_2O-Ar system has recently been

developed by fitting high-level ab initio data calculated at the frozen-core (FC) explicitly correlated coupled cluster singles, doubles and perturbative triples [FC-CCSD(T)-F12a] level, with the augmented correlation-consistent polarized valence quadruple-zeta basis set plus bond functions.[28] The fitting was done with the permutation-invariant polynomial neural network (PIP-NN) method,[30] in which the PIPs enforce the permutation symmetry between the two identical H nuclei while the NN providing a highly flexible functional form. The fitting root-mean square error is 0.284 cm^{-1}, underscoring high fitting fidelity.

For the quantum scattering calculations, we chose to work with the Radau-Jacobi hybrid coordinates $(R, r_1, r_2, \theta_1, \theta_2, \phi)$, as shown in Figure 1, which was first introduced in a publication by Brocks et al.[31] The computational details of the TIQM scattering calculations can be found in Ref. [16], so only a brief introduction is given here. First, the eigenfunctions of the ro-vibrational H_2O Hamiltonian were determined and then used as a contracted basis to expand the total scattering wavefunction. With the basis functions substituted into the TI Schrödinger equation, the close-coupling equations were constructed, which were then solved by a log-derivative method[32, 33] to obtain the scattering matrix and the *L*-summed state-to-state transition probability $P_{f \leftarrow i}$, where *i*/*f* represents an initial/final MIS. We stress that the scattering wave function and the basis functions are all parity adapted, which not only reduced the dimensionality of the problem, but also forbade transitions between *para*- and *ortho*-states of H_2O, as dictated by the conservation of nuclear spins.

The state-to-state integral cross section (ICS) was calculated in terms of $P_{f \leftarrow i}$,

$$\sigma_{f\leftarrow i}\left(E_{\mathrm{c}}\right)=\frac{\pi}{\left(2j_i+1\right)2\mu E_{\mathrm{c}}}\sum_{J}\left(2J+1\right)P^{J}_{f\leftarrow i}\left(E_{\mathrm{c}}\right). \tag{2}$$

Here, μ is the reduced mass of the H_2O+Ar system, j_i is the rotational quantum number associated with the initial MIS i, J is the total angular momentum quantum number, and E_{c} is the collision energy. The state-to-state rate coefficient as a function of temperature T was obtain as follows

$$k_{f\leftarrow i}\left(T\right)=\frac{1}{k_{\mathrm{B}}T}\sqrt{\frac{8}{\pi\mu k_{\mathrm{B}}T}}\int_0^{\infty}\sigma_{f\leftarrow i}\left(E_{\mathrm{c}}\right)E_{\mathrm{c}}\exp\left(-E_{\mathrm{c}}/k_{\mathrm{B}}T\right)\mathrm{d}E_{\mathrm{c}}, \tag{3}$$

where k_{B} is Boltzmann constant. The rate coefficient from the initial MIS i to the final vibrational state v' was calculated by summing over all corresponding final MISs f belonging to the final state v',

$$k_{v'\leftarrow i}\left(T\right)=\sum_{f}^{f\in v'}k_{f\leftarrow i}\left(T\right). \tag{4}$$

In order to directly compare with experimental results, the vibrational state specific rate coefficient from the initial vibrational state v to the final vibrational state v' was calculated by further averaging over all corresponding initial MISs,

$$k_{v'\leftarrow v}\left(T\right)=\frac{\sum_{i}^{i\in v}w_i k_{v'\leftarrow i}\left(T\right)}{\sum_{i}^{i\in v}w_i}. \tag{5}$$

Here, the Boltzmann weighting factor is $w_i=\left(2j_i+1\right)\exp\left(-E_{\mathrm{int},i}/k_{\mathrm{B}}T\right)$ for *para*-H_2O and $w_i=3\left(2j_i+1\right)\exp\left(-E_{\mathrm{int},i}/k_{\mathrm{B}}T\right)$ for *ortho*-H_2O, respectively, where $E_{\mathrm{int},i}$ is the internal energy of initial MIS i. Note that three quantum numbers $\left(v_1,v_2,v_3\right)$ label a vibrational state v/v' in these equations above. Atomic units are used throughout the

paper unless specifically pointed out.

Extensive convergence tests were performed to determine the numerical parameters of the scattering calculations. The number of potential optimized discrete variable representation (PODVR)[34] points were chosen as $N_{r_1} = N_{r_2} = 4$. The numbers of points in θ_1, θ_2, and ϕ coordinates were $N_{\theta_1} = 29$, $N_{\theta_2} = 25$, and $N_{\phi} = 23$, respectively. The energy truncation for the contracted basis functions employed in all the calculations was $E_{\text{int, max}}$=6000 cm^{-1}, which corresponds to the maximum values of the rotational quantum number: j_{max}=22, 18, 13, 11, 11, and 4 for vibrational states (0, 0, 0), (0, 1, 0), (0, 2, 0), (1, 0, 0), (0, 0, 1) and (0, 3, 0), respectively Additionally, considering the stretching modes were the main focus, we have added a few extra rotational basis functions for states (2, 0, 0) and (0, 0, 2), namely, j_{max}=3 and 2, respectively, although their internal energies already exceed 7000 cm^{-1}. The maximum total angular momentum quantum number was set to be J_{max}=200, which is sufficient to converge the ICSs in the energy range of interest. Furthermore, the log-derivative propagation was carried out with different step sizes ΔR in different ranges of R: ΔR=0.01 a_0 in $R \in$ [4.0, 7.0] a_0, ΔR=0.02 a_0 in $R \in$ [7.0, 12.0] a_0, and ΔR=0.04 a_0 in $R \in$ [12.0, 20.0] a_0. The state-to-state transition probabilities were found to change no more than 1% when propagating to a larger distance of R=24.0 a_0, suggesting good convergence with respect to the propagation length.

3. Results

We first focus on the initial vibrational state (0, 0, 1) of H_2O, which is the first excited state for the antisymmetric stretch mode. Figure 2 shows the state-to-state ICSs in log scale for two selected initial MISs associated with this vibrational state as a function of the internal energy difference between final and initial MISs (i.e., $E_{\text{diff}} = E_{\text{int},f} - E_{\text{int},i}$) at several collision energies. All corresponding final ro-vibrational states in the inelastic collision are shown in each panel and color coded by their final vibrational states. The vertical black lines represent zero internal energy difference.

In the current system, the scattering into different final vibrational states clearly shows a propensity for the energy gap law.[10] Figure 2 revealed this clear trend in the magnitude of inelastic scattering ICSs for different final vibrational states, decreasing in the order (0, 0, 1) > (1, 0, 0) > (0, 2, 0) > (0, 1, 0) > (0, 0, 0). The scattering into the (0, 0, 1) product state, when possible, corresponds to pure rotationally inelastic scattering, which not surprisingly has the largest probability among all final vibrational states. The scattering into the (1, 0, 0) state has the second largest ICSs, because this vibrational state has the nearest internal energy to the initial vibrational state among all vibrationally inelastic channels. For the bending excited final state, the (0, 2, 0) state has a closer internal energy to the initial (0, 0, 1) state than (0, 1, 0), thus larger ICSs. Finally, the ground vibrational state (0, 0, 0), has the smallest ICSs, due to its largest energy gap with the initial state. Within each specific final vibrational manifold, the ICSs are also dominated by those MISs whose internal energies are nearest to those of the initial MIS, apparently also dictated by the energy gap law.[10]

We emphasize that the energy gap law is observed for all collision energies studied here from 10 to 1000 cm^{-1}. This situation differs from our previous work on the vibrational quenching of H_2O by Cl atoms, where the energy gap law gradually breaks down for collision energies above 600 cm^{-1}.[16] The different behaviors between two systems (H_2O+Cl and H_2O+Ar) can be explained by the different strengths of interaction. The interaction potential well between H_2O and Cl is ~1300 cm^{-1},[35] which is much deeper than the current system H_2O+Ar of ~140 cm^{-1}.[36] For collision energies above 600 cm^{-1}, high partial wave collisions dominate and a long lived [ClH_2O] intermedium complex is formed during the scattering process, which leads to facile intramolecular vibrational energy redistribution (IVR). Under such circumstances, memory of the initial MIS is quickly lost and that energy gap law breaks down.[15] We note in passing that the self-relaxation of vibrationally excited H_2O is known to be extremely efficient,[18] specially at low temperatures, thanks to the strong hydrogen bond interactions. On the other hand, for H_2O+Ar, the shallow van der Waals well makes it difficult to support such a long-lived intermedium complex and the direct collision mechanism is always dominant, which upholds the energy gap law in the entire energy range studied here. Under such circumstances, the scattering is dominated by repulsive wall.

We also noticed that in Figure 2 (d)-(f), although there exist many MISs associated with the vibrational ground (0, 0, 0) state whose internal energies are near to that of the initial MIS (0, 0, 1) $0_{0,0}$ of 3745 cm^{-1}, (for example, (0, 0, 0) $12_{12,1}$ at 3743 cm^{-1}), their

corresponding ICSs are still rather small. For the (0, 0, 0) $12_{12,1} \leftarrow$(0, 0, 1) $0_{0,0}$ transition, for example, the change of the rotational quantum number is quite significant: Δj=12. On the other hand, states with small j values, which are distributed with the most negative E_{diff}, have generally larger ICSs than those with larger j values. These trends can be attributed to angular momentum gap law,[14] even when the energy gap law is satisfied. This trend is generally observed by direct collision scattering processes, such as Ar+HF,[37] H_2+H_2,[38-40] H_2+CO,[41, 42] and H_2+CN,[43] but it is a weaker gap law than that based on the energy gap. Furthermore, vibrational wavefunctions of states (0, 0, 0) and (0, 0, 1) are also weakly coupled. Therefore, ICSs for transitions of this type are all strongly suppressed because of all above factors combined.

The state-to-state rate coefficients, as defined in Eq. (3), are shown in Figure 3 for transitions $(1,0,0)\, j'_{k'_a,k'_c} \leftarrow (0,0,1) 1_{0,1}$ and $(1,0,0)\, j'_{k'_a,k'_c} \leftarrow (0,0,1) 0_{0,0}$, which are respectively exemplars for *para*- and *ortho*-H_2O. Their temperature dependences are marked in the figure by solid and dashed lines for exothermic and endothermic transitions, respectively. The internal energies for these participating MISs can be found in Table 1. It is clearly seen that the rate coefficients for exothermic transitions are either independent of the temperature or decrease very slowly with temperatures. For endothermic transitions with large internal energy differences between final and initial MISs, rate coefficients increase with temperature rapidly at low temperatures, while the increase slows down at high temperatures. It is particularly interesting that the rate coefficients for near-resonant transitions, which are defined here by internal energy

differences (of absolute value) less than 20 cm^{-1}, are always dominant, as shown for the final MIS (1, 0, 0) $3_{1,3}$ in Figure 3 (a) and (1, 0, 0) $2_{1,2}$ in Figure 3 (b). This is another manifestation of the energy gap law. For these two near-resonant energy transfer processes, the rate coefficients are almost independent of the temperature.

The vibrational state specific rate coefficients, defined by Eq. (5), are shown in Figure 4 for the (0, 0, 1), (1, 0, 0) and (0, 2, 0) initial states. Again, in Figure 4 (a), for the (0, 0, 1) initial state, the final state resolved rate coefficients rank as (1, 0, 0) > (0, 2, 0) > (0, 1, 0) > (0, 0, 0), while they rank as (0, 0, 1) > (0, 2, 0) > (0, 1, 0) > (0, 0, 0) for the (1, 0, 0) initial state in Figure 4 (b). As we discussed above, these rate coefficients all observe the energy gap law. In Figure 4 (c) for the (0, 2, 0) initial state, the rate coefficient for the final state (0, 1, 0) dominates the at low temperatures, while at higher temperatures, rate coefficients for the final states (0, 1, 0), (1, 0, 0), and (0, 0, 1) have roughly the same order of magnitude, e.g., 10^{-13} $cm^3s^{-1}mol^{-1}$ at 500 K. As shown in Table 1, transitions from the (0, 2, 0) state to two stretching fundamentals, (0, 0, 1) and (1, 0, 0), are both endothermic, which leads to the strong suppression of the corresponding thermal rate coefficients at low temperatures. As the temperature increases from 50 to 500 K, they quickly increase by five orders of magnitude. Finally, transitions to the (0, 0, 0) final state are always the least probable and the corresponding rate coefficient is three orders of magnitude smaller than that to (0, 1, 0) at all temperatures.

The total vibrational relaxation rate coefficients for the combined stretching fundamental state (0, 0, 1)/(1, 0, 0) and for the bending overtone state (0, 2, 0) as initial

states are shown in Figure 5, together with available experimental results.[18, 19, 21] In these experiments, the two stretching states (0, 0, 1) and (1, 0, 0) were treated as a single reservoir state. In order to compare with the experimental results directly, the total vibrational relaxation rate coefficients for the combined stretching fundamental (0, 0, 1)/(1, 0, 0) were calculated by Boltzmann-averaging the total relaxation rate coefficients for the individual (0, 0, 1) and (1, 0, 0) states, which were respectively obtained by summing over all thermally accessible final states in the (0, 2, 0), (0, 1, 0), and (0, 0, 0) vibrational manifolds. Likewise, those for the initial state (0, 2, 0) were obtained by including all vibrationally inelastic final states, whether they correspond to either relaxation or excitation channels.

As shown in the figure, the calculated thermal rate coefficient for the relaxation of the combined (0, 0, 1)/(1, 0, 0) state increases monotonously in the temperature range from 20 to 500 K. This tendency is consistent with the experimental results by Hovis et al.[19] At room temperature T=295 K, our results of 1.52×10^{-13} $cm^3s^{-1}mol^{-1}$ is in very good agreement with the experimental one of $(1.4\pm0.2)\times10^{-13}$ $cm^3s^{-1}mol^{-1}$ by Finzi et al.,[18] and consistent with the upper limit reported by Zittel and Masturzo.[21] For the (0, 2, 0) initial state, the total vibrational relaxation rate coefficient also increases with temperature, which is also consistent with the data of Hovis et al.[19] However, Finzi et al. reported a value of $(4.2\pm0.9)\times10^{-13}$ $cm^3s^{-1}mol^{-1}$ at the room temperature,[18] which is over five times larger than our value of 7.8×10^{-14} $cm^3s^{-1}mol^{-1}$. Our calculation result is significantly lower than the upper limit of Zittel and Masturzo.[21]

4. Discussion

As discussed in Introduction, the two state-resolved experiments from the Moore group all used a kinetic model to fit the LIF measurements of population decay.[18, 19] Specifically, several water-argon mixtures with different partial pressures were first prepared. The water molecules were then excited to individual ro-vibrational states in the antisymmetric stretching fundamental (0, 0, 1) band by an IR laser. Intensities of fluorescence from both the (0, 0, 1) and (0, 2, 0) states were monitored as a function of time, which provided the kinetic traces. To fit the kinetic traces, a kinetic model for energy transfer among the relevant vibrational states was constructed as follows. First, a very fast thermal equilibrium between (0, 0, 1) and (1, 0, 0) states was assumed, because of the small energy gap between the two. The following "equilibrium constant" was defined in their kinetical modelling of the LIF traces:[18]

$$\beta \equiv \frac{k_{-}(T)}{k_{+}(T)} = \frac{g_{+}}{g_{-}} \exp\left(-\frac{E_{\mathrm{int},+} - E_{\mathrm{int},-}}{k_{\mathrm{B}} T} \right), \qquad (6)$$

where g_{+}/g_{-} is the degeneracy of the initial state and for vibrational states g=1. Here, the (1, 0, 0)←(0, 0, 1) and (0, 0, 1)←(1, 0, 0) transitions are defined as the forward (+) and backward (-) directions. The stretching states were thus regarded as a reservoir state (0, 0, 1)/(1, 0, 0), which is assumed to relax to the (0, 2, 0) state as the primary energy transfer process. This process is assumed to be much slower than the mixing of the two stretching states. The corresponding total relaxation rate coefficient for the combined (0, 0, 1)/(1, 0, 0) state was obtained by fitting kinetic parameters which reflects the kinetic trace of the

(0, 0, 1) fluorescence intensity. The relaxation from the (0, 2, 0) to (0, 1, 0) state was considered as the secondary process and only the (0, 1, 0) and (0, 0, 0) states were treated as the relaxation products of the (0, 2, 0) state.

We note that the relaxation rate coefficients of the (0, 2, 0) initial state reported in these experiments are larger than those of the (0, 0, 1)/(1, 0, 0) state, respectively, which is sharp contrast with our computational results. We attribute this theory-experiment disagreement to several approximations introduced in the kinetic model employed to fit the LIF traces. As we mentioned above, the assumption of a single reservoir state of the stretching fundamentals (0, 0, 1)/(1, 0, 0) strongly relied on the precondition of very fast equilibration of the two stretching fundamental states. Finzi et al. stated that their kinetic model is valid when the rate coefficient of transition (1, 0, 0)←(0, 0, 1) at 298 K is greater than 2.93×10^{-10} $cm^3s^{-1}mol^{-1}$. This condition is apparently not satisfied as our calculated result is twenty times smaller, at 1.24×10^{-11} $cm^3s^{-1}mol^{-1}$, as shown in Figure 4. They also used an equilibrium estimation of the β value 0.64 by Eq. (6), which deviates from our calculated value of 0.82. We note that because the decay of the combined (0, 0, 1)/(1, 0, 0) state is the primary event in the kinetic model, and the corresponding rates are presumably better constrained. Thus, we are satisfied by the good agreement with the rate coefficients derived from the experimental measurements. However, we believe that the experimental relaxation rate coefficients for the (0, 2, 0) state are probably much more uncertain because it is a secondary kinetic event, which not only depends on the population transfer from the higher (0, 0, 1)/(1, 0, 0) states, but also relaxation to lower

(0, 1, 0) and (0, 0, 0) states. Furthermore, as shown in Figure 4, we note that the (0, 0, 1)/(1, 0, 0)←(0, 2, 0) transitions are as efficient as the (0, 1, 0)←(0, 2, 0) one at 298 K, although the latter dominates at lower temperatures. This is because the energy gap between the former states is much smaller than that for the latter one, and both stretching fundamentals are thermally accessible at the room temperature. This vibrational excitation process was completely neglected in the kinetic model. Although these approximations in the kinetic model were made with reasonable assumptions, our quantum state-to-state rate coefficients have clearly pointed out their potential inadequacy in the current system. Their impact on the extracted rate coefficients, particularly the secondary process of the (0, 2, 0) relaxation, is difficult to quantify, but certainly needs be scrutinized further in the future, perhaps with more sophisticated experimental techniques. If the theoretical predictions are proven correct, changes need be made in kinetic models involving vibrational relaxation of water.

5. Conclusions

For the first time, we report in this work exact quantum scattering calculations of ro-vibrational energy transfer dynamics for H_2O in collision with Ar, using an accurate full-dimensional PES. For the (0, 0, 1) initial state, clear trends in the magnitude of inelastic scattering ICSs are found, with the final state specific rate coefficient decreasing in the order (0, 0, 1) > (1, 0, 0) > (0, 2, 0) > (0, 1, 0) > (0, 0, 0) by the final state. This tendency shows that the energy transfer dynamics in the current system is clearly governed by the energy gap law. The transitions between two stretching fundamental

states (1, 0, 0)↔(0, 0, 1) are the most efficient one in all vibrationally inelastic transitions, thanks to the small energy gap between the two vibrational states. Within each vibrational manifold, the energy gap law is also observed. All of the state-to-state and total rate coefficients for transitions from initial states (1, 0, 0), (0, 0, 1) and (0, 2, 0) are also shown to closely follow the energy gap law. The clear observance of the energy gap law is attributable to the weak interaction between the collision partners in the current system, for which the collision is largely dominated by repulsive walls.

The relaxation rate coefficients for the (0, 0, 1)/(1, 0, 0) and (0, 2, 0) initial states were further calculated and compared with available experiment results. Our calculated results for the relaxation of the stretching fundamentals are in good agreement with experimentally extracted rate coefficients, but those for the bending overtone are much larger than the measured ones. Considering the self-consistency of theoretical calculations, we attribute this theory-experiment discrepancy to the approximations used in the kinetic model to extract the experimental rate coefficients. Evidence is present to show the inadequacy of these approximations. Further quantum state resolved experimental studies are needed to resolve this controversy.

Acknowledgements: This work was supported by the Department of Energy (DE-SC0015997 to H. G.) and in part by the National Natural Science Foundation of China (Grant No. 21733006 to DX). The calculations were performed at High Performance Computing Center (HPCC) at NJU and Center for Advanced Research

Computing (CARC) at UNM.

References

1. J. R. Barker, *Progress and Problems in Atomspheric Chemistry*, World Scientific, Singapore, 1995.
2. A. W. Jasper, *J. Phys. Chem. A*, 2020, **124**, 1205-1226.
3. E. Roueff and F. Lique, *Chem. Rev.*, 2013, **113**, 8906-8938.
4. M. C. Lin, M. E. Umstead and N. Djeu, *Annu. Rev. Phys. Chem.*, 1983, **34**, 557-591.
5. S. H. Robertson, ed. *Unimolecular Kinetics: Parts 2 and 3: Collisional Energy Transfer and the Master Equation*, Elsevier2019.
6. G. W. Flynn, C. S. Parmenter and A. M. Wodtke, *J. Phys. Chem.*, 1996, **100**, 12817-12838.
7. G. Lendvay and G. C. Schatz, in *Unimolecular Kinetics: Parts 2 and 3: Collisional Energy Transfer and the Master Equation*, ed. S. H. Robertson, Elsevier2019.
8. G. Lendvay, in *Unimolecular Kinetics: Parts 2 and 3: Collisional Energy Transfer and the Master Equation*, ed. S. H. Robertson, Elsevier2019.
9. D. Babikov and A. Semenov, *J. Phys. Chem. A*, 2016, **120**, 319-331.
10. A. J. McCaffery, *Phil. Trans. Royal Soc. A*, 2018, **376**, 20170150.
11. J. C. Polanyi and K. B. Woodall, *J. Chem. Phys.*, 1972, **56**, 1563-1572.
12. B. Stewart, P. D. Magill, T. P. Scott, J. Derouard and D. E. Pritchard, *Phys. Rev. Lett.*,

1988, **60**, 282-285.

13. J. A. Mack, K. Mikulecky and A. M. Wodtke, *J. Chem. Phys.*, 1996, **105**, 4105-4116.

14. A. J. McCaffery, M. A. Osborne, R. J. Marsh, W. D. Lawrance and E. R. Waclawik, *J. Chem. Phys.*, 2004, **121**, 169-180.

15. D. Yang, J. Huang, X. Hu, H. Guo and D. Xie, *Nat. Commun.*, 2019, **10**, 4658.

16. D. Yang, D. Xie and H. Guo, *J. Phys. Chem. A*, 2021, **125**, 6864-6871.

17. R. O. Manuilova, A. G. Feofilov, A. A. Kutepov and V. A. Yankovsky, *Adv. Space Res.*, 2015, **56**, 1806-1814.

18. J. Finzi, F. E. Hovis, V. N. Panfilov, P. Hess and C. B. Moore, *J. Chem. Phys.*, 1977, **67**, 4053-4061.

19. F. E. Hovis and C. B. Moore, *J. Chem. Phys.*, 1980, **72**, 2397-2402.

20. Š. S. Miljanic and C. B. Moore, *J. Chem. Phys.*, 1980, **73**, 226-229.

21. P. F. Zittel and D. E. Masturzo, *J. Chem. Phys.*, 1989, **90**, 977-989.

22. P. W. Barnes, I. R. Sims and I. W. M. Smith, *J. Chem. Phys.*, 2004, **120**, 5592-5600.

23. J. Ree and H. K. Shin, *Chem. Phys. Lett.*, 1989, **163**, 308-314.

24. J. Ree and H. K. Shin, *Chem. Phys. Lett.*, 1990, **167**, 220-226.

25. J. Ree and H. K. Shin, *J. Chem. Phys.*, 1990, **93**, 6463-6472.

26. J. Ree and H. K. Shin, *Chem. Phys. Lett.*, 1992, **193**, 215-224.

27. D. Yang, D. Xie and H. Guo, *J. Phys. Chem. Lett.*, 2022, **13**, 1777-1784.

28. Q. Liu, J. Wang, Y. Zhou and D. Xie, *Curr. Chin. Sci.*, in press.

29. B. Jiang, D. Xie and H. Guo, *J. Chem. Phys.*, 2012, **136**, 034302.

30. B. Jiang, J. Li and H. Guo, *Int. Rev. Phys. Chem.*, 2016, **35**, 479-506.

31. G. Brocks, A. van der Avoird, B. T. Sutcliffe and J. Tennyson, *Mole. Phys.*, 1983, **50**, 1025-1043.

32. B. R. Johnson, *J. Comput. Phys.*, 1973, **13**, 445-449.

33. D. E. Manolopoulos, *J. Chem. Phys.*, 1986, **85**, 6425-6429.

34. J. Echave and D. C. Clary, *Chem. Phys. Lett.*, 1992, **190**, 225-230.

35. J. Li, R. Dawes and H. Guo, *J. Chem. Phys.*, 2013, **139**, 074302.

36. D. Hou, Y.-T. Ma, X.-L. Zhang and H. Li, *J. Chem. Phys.*, 2016, **144**, 014301.

37. D.-z. Yang, Q. Liu, H.-l. Zhao and D.-q. Xie, *Chin. J. Chem. Phys.*, 2019, **32**, 67-71.

38. G. Quéméner and N. Balakrishnan, *J. Chem. Phys.*, 2009, **130**, 114303.

39. S. F. d. Santos, N. Balakrishnan, S. Lepp, G. Quéméner, R. C. Forrey, R. J. Hinde and P. C. Stancil, *J. Chem. Phys.*, 2011, **134**, 214303.

40. S. F. d. Santos, N. Balakrishnan, R. C. Forrey and P. C. Stancil, *J. Chem. Phys.*, 2013, **138**, 104302.

41. B. Yang, P. Zhang, X. Wang, P. C. Stancil, J. M. Bowman, N. Balakrishnan and R. C. Forrey, *Nat. Comm.*, 2015, **6**, 6629.

42. B. Yang, N. Balakrishnan, P. Zhang, X. Wang, J. M. Bowman, R. C. Forrey and P. C. Stancil, *J. Chem. Phys.*, 2016, **145**, 034308.

43. B. Yang, X. H. Wang, P. C. Stancil, J. M. Bowman, N. Balakrishnan and R. C. Forrey, *J.*

Chem. Phys., 2016, **145**, 224307.

44. J. Tennyson, N. F. Zobov, R. Williamson, O. L. Polyansky and P. F. Bernath, *J. Phys. Chem. Ref. Data*, 2001, **30**, 735-831.

Table 1. Calculated eigenenergy of some MISs of the H_2O molecule using the PES of Jiang et al.[29] and comparison with the experimental data.[44] Energies are given in cm^{-1}.

(v_1, v_2, v_3)	j_{k_a,k_c}	This work	Expt.	(v_1, v_2, v_3)	j_{k_a,k_c}	This work	Expt.
para-H_2O				*ortho*-H_2O			
(0, 0, 0)	$0_{0,0}$	0	0	(0, 0, 0)	$1_{0,1}$	23.7	23.8
(0, 1, 0)	$0_{0,0}$	1595.5	1594.7	(0, 1, 0)	$1_{0,1}$	1619.2	1618.6
(0, 2, 0)	$0_{0,0}$	3153.8	3151.6	(0, 2, 0)	$1_{0,1}$	3177.6	3175.4
(1, 0, 0)	$0_{0,0}$	3647.8	3657.0	(1, 0, 0)	$1_{0,1}$	3671.1	3680.4
	$1_{1,1}$	3683.8	3693.3		$1_{1,0}$	3689.0	3698.5
	$2_{0,2}$	3716.5	3725.9		$2_{1,2}$	3725.3	3734.9
	$2_{1,1}$	3740.9	3750.5		$2_{2,1}$	3778.6	3788.7
	$2_{2,0}$	3779.9	3789.9		$3_{0,3}$	3781.7	3791.4
	$3_{1,3}$	3786.8	3796.5		$3_{1,2}$	3817.6	3827.4
	$4_{2,2}$	3956.2	3966.6		$3_{2,1}$	3854.6	3864.8
	$5_{3,3}$	4138.8	4150.3		$3_{3,0}$	3924.3	3935.3
(0, 0, 1)	$1_{0,1}$	3768.3	3779.5	(0, 0, 1)	$0_{0,0}$	3744.8	3755.9
	$3_{1,2}$	3915.2	3926.9		$3_{2,2}$	3944.6	3956.7

Figure 1. Scattering coordinates $(R, r_1, r_2, \theta_1, \theta_2, \phi)$ used for the H_2O+Ar system.

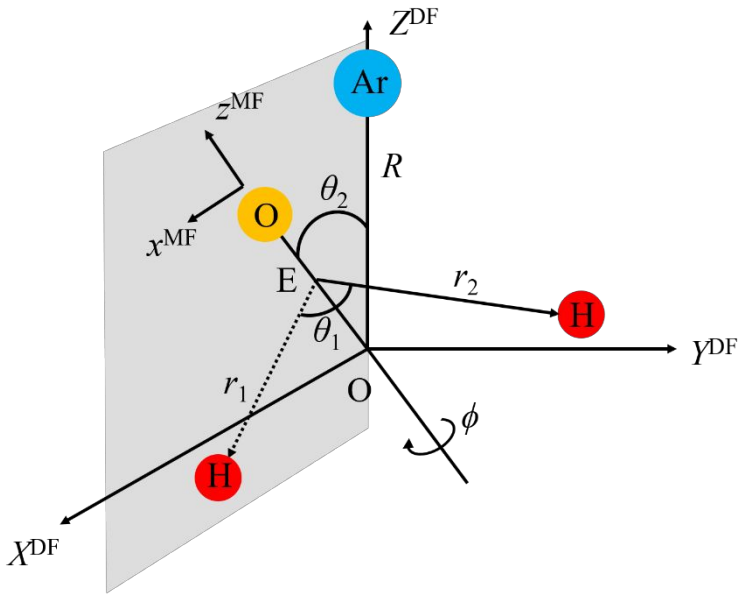

Figure 2. Calculated state-to-state inelastic ICSs for several initial rotational states of H_2O (0, 0, 1) as a function of internal energy difference (E_{diff}). The final vibrational states are color coded and black line is for zero internal energy difference.

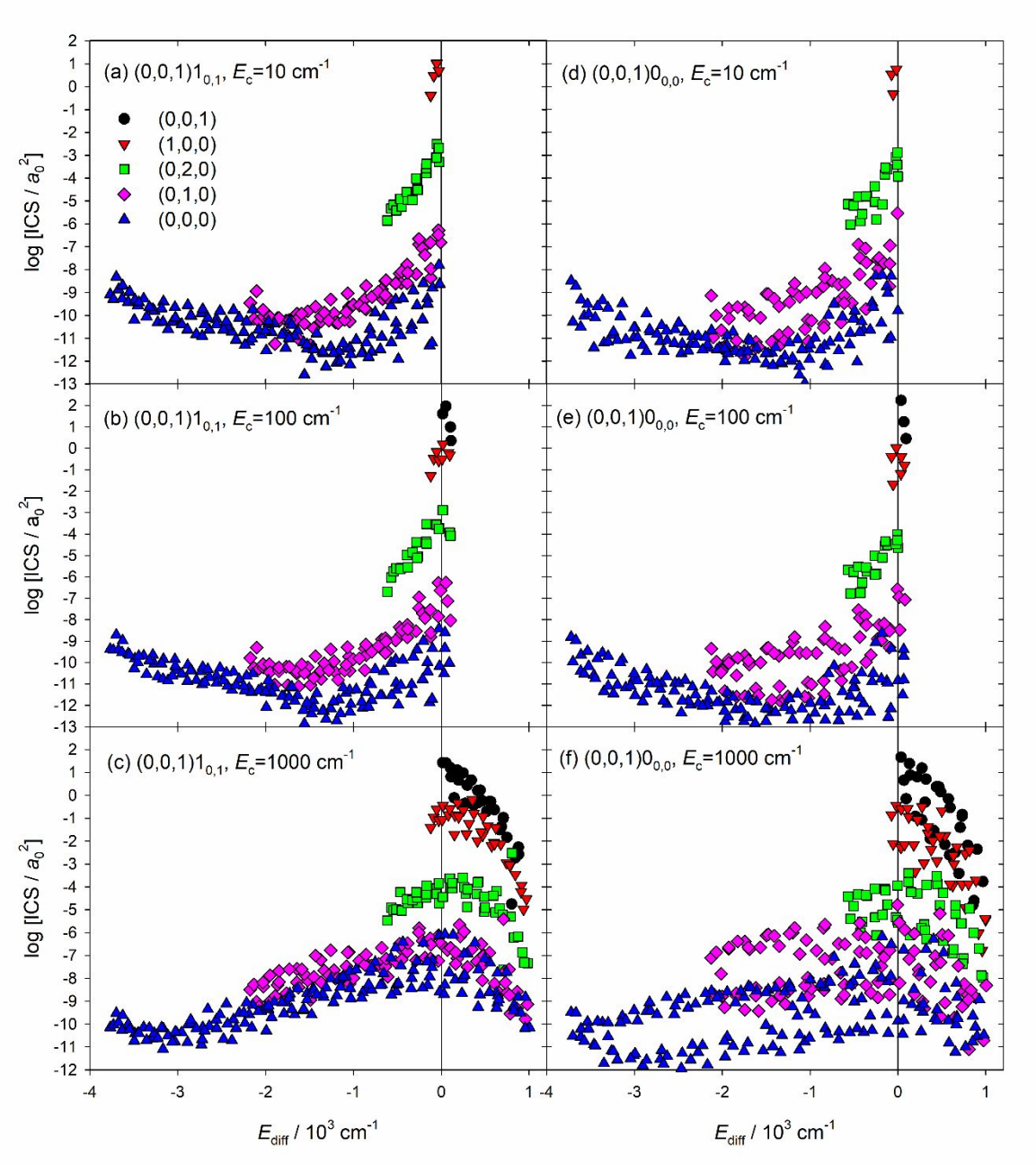

Figure 3. Calculated state-to-state rate coefficients for the (1, 0, 0)←(0, 0, 1) transition as a function of temperature for two initial rotational states of H_2O.

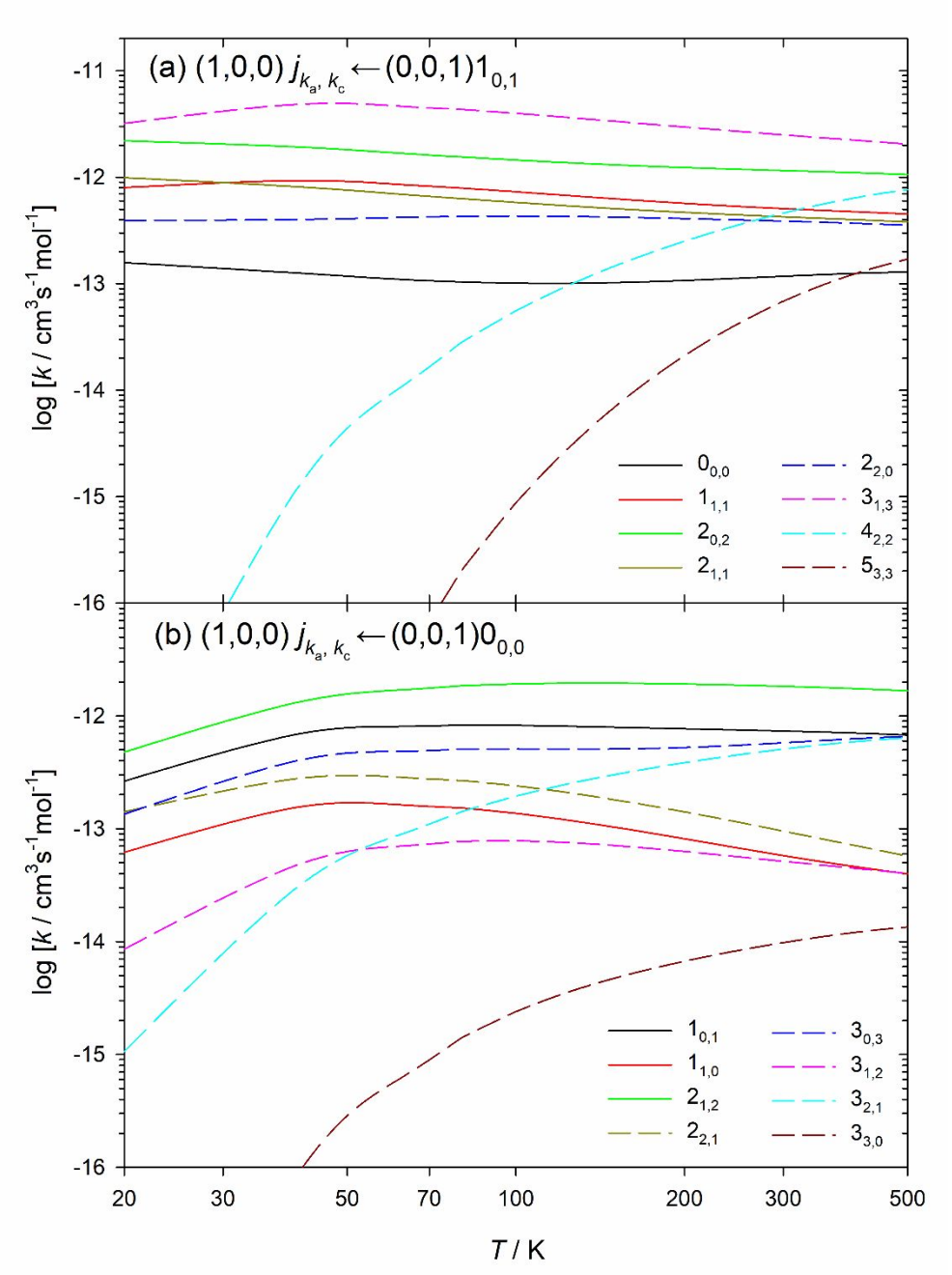

Figure 4. Calculated vibrationally inelastic state-to-state rate coefficients as a function of temperature from the (0, 0, 1) [panel (a)] (1, 0, 0) [panel (b)], and (0, 2, 0) [panel (c)] initial states.

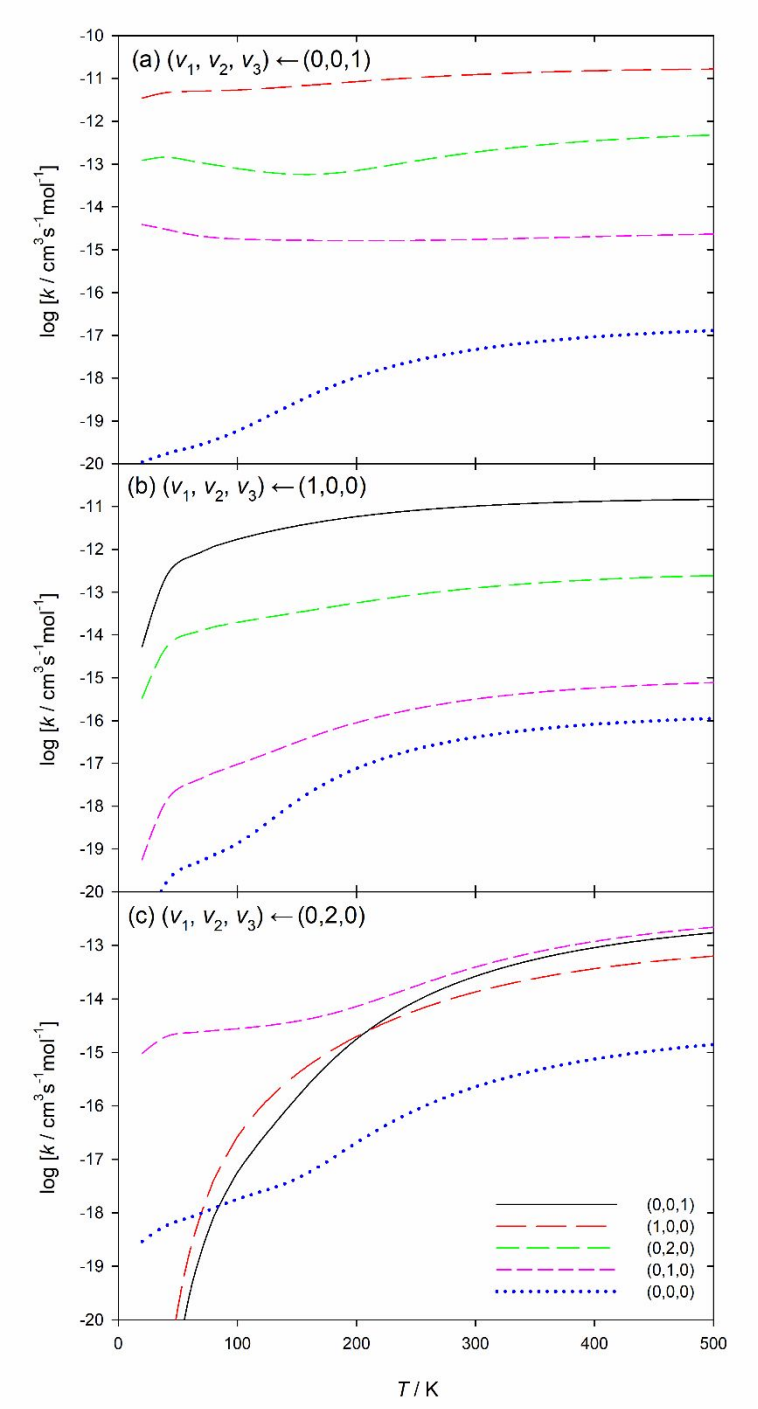

Figure 5. Comparison of theoretical and experimental state-resolved total vibrational relaxation thermal rate coefficients for the combined stretching fundamental state (0, 0, 1)/(1, 0, 0) and bending overtone (0, 2, 0) state. The rate coefficients for the stretching fundamental state calculated in this work were obtained by Boltzmann-averaging those for the symmetric and antisymmetric stretching states.